Circulation

ORIGINAL RESEARCH ARTICLE

Immunothrombotic Dysregulation in COVID-19 Pneumonia Is Associated With Respiratory Failure and Coagulopathy

BACKGROUND: Severe acute respiratory syndrome corona virus 2 infection causes severe pneumonia (coronavirus disease 2019 [COVID-19]), but the mechanisms of subsequent respiratory failure and complicating renal and myocardial involvement are poorly understood. In addition, a systemic prothrombotic phenotype has been reported in patients with COVID-19.

METHODS: A total of 62 subjects were included in our study (n=38 patients with reverse transcriptase polymerase chain reaction–confirmed COVID-19 and n=24 non–COVID-19 controls). We performed histopathologic assessment of autopsy cases, surface marker–based phenotyping of neutrophils and platelets, and functional assays for platelet, neutrophil functions, and coagulation tests, as well.

RESULTS: We provide evidence that organ involvement and prothrombotic features in COVID-19 are linked by immunothrombosis. We show that, in COVID-19, inflammatory microvascular thrombi are present in the lung, kidney, and heart, containing neutrophil extracellular traps associated with platelets and fibrin. Patients with COVID-19 also present with neutrophil-platelet aggregates and a distinct neutrophil and platelet activation pattern in blood, which changes with disease severity. Whereas cases of intermediate severity show an exhausted platelet and hyporeactive neutrophil phenotype, patients severely affected with COVID-19 are characterized by excessive platelet and neutrophil activation in comparison with healthy controls and non–COVID-19 pneumonia. Dysregulated immunothrombosis in severe acute respiratory syndrome corona virus 2 pneumonia is linked to both acute respiratory distress syndrome and systemic hypercoagulability.

CONCLUSIONS: Taken together, our data point to immunothrombotic dysregulation as a key marker of disease severity in COVID-19. Further work is necessary to determine the role of immunothrombosis in COVID-19.

Leo Nicolai, MD*
Alexander Leunig, BA*
⋮
Kami Pekayvaz, MD†
Konstantin Stark, MD†

*Dr Nicolai and A. Leunig contributed equally

†Drs Pekayvaz and Stark contributed equally.

The full author list is available on page 1187.

Key Words: blood platelets ■ COVID-19 ■ disseminated intravascular coagulation ■ neutrophils ■ respiratory insufficiency ■ severe acute respiratory syndrome coronavirus 2 ■ thrombosis

Sources of Funding, see page 1187

https://www.ahajournals.org/journal/circ

Clinical Perspective

What Is New?

- Dysregulated platelets and neutrophils cooperate to drive a systemic prothrombotic state in severe acute respiratory syndrome corona virus 2 infection, indicating inflammation as a trigger for thrombotic complications frequently observed during coronavirus disease 2019 (COVID-19).
- Microvascular thrombi containing neutrophils, platelets, and neutrophil extracellular traps are a hallmark of severe acute respiratory syndrome corona virus 2 infection, linking multiorgan failure and systemic hypercoagulability in COVID-19.

What Are the Clinical Implications?

- Severe acute respiratory syndrome corona virus 2–infected patients are at increased risk for thrombotic events, making prophylactic anticoagulation and vigilant monitoring for thrombotic complications a central task in management of patients with COVID-19.
- Targeting immunothrombosis or neutrophil extracellular trap formation by modulating platelet-neutrophil interactions could be a valuable therapeutic approach for respiratory failure and thrombotic complications in COVID-19.

The coronavirus disease 2019 (COVID-19) pandemic is a global healthcare challenge, with rapid spread, high contagiousness, and an approximate case fatality rate of 1.0% to 2.3%.[1–4] However, because of the lack of specific treatment, therapy has so far been limited mainly to supportive care.[4–6]

Although acute respiratory distress syndrome is the central feature of disease severity, nonpulmonary organ damage has emerged as an important predictor of mortality.[7] Patients hospitalized for COVID-19 are at high risk for kidney failure, and myocardial involvement is common in severe cases, both correlating with poor outcome.[8–10] The underlying mechanisms of COVID-19 pulmonary and nonpulmonary tissue injury are insufficiently understood.[11]

Preliminary data point to a prothrombotic state in patients with COVID-19,[12] with a possible beneficial effect of heparin. However, a thorough analysis of cellular and plasmatic coagulation of affected patients is missing.[13–15] In particular, it is unclear whether and how the inflammatory response to severe acute respiratory syndrome corona virus 2 (SARS-CoV-2) and its associated coagulopathy are intertwined. Recent evidence from translational and basic research has established the concept of immunothrombosis, a process that integrates innate immunity, platelets, and clotting factors to capture and fight invading pathogens but also contributes to inflammation-related tissue damage.[16,17]

In this study, we provide first evidence that neutrophils, immunogenic platelets, and a dysregulated coagulation cascade cooperate to propagate immunothrombotic tissue injury in COVID-19, as shown in autopsy specimens and the blood of patients. Our data show distinct neutrophil and platelet activation states and increased plasmatic coagulation in COVID-19, all of which correlate with disease progression. Therefore, immunothrombosis is not only a bystander in COVID-19, but represents a central pathogenic factor linking respiratory failure and systemic hypercoagulability.

METHODS

Cohort

The data that support the findings of this study are available from the corresponding author on reasonable request. A total of 62 subjects were included in our study (n=38 patients with reverse transcriptase polymerase chain reaction–confirmed COVID-19 and n=24 non–COVID-19 control groups). The study design is outlined in (Figure IA through IE in the Data Supplement). Patients with severe preexisting kidney or liver dysfunction, severe autoimmune diseases, immunosuppression, chronic infection, patients requiring extracorporeal membrane oxygenation therapy, with a known coinfection with influenza or respiratory syncytial virus, and patients receiving antiplatelet medication were excluded. Patients with COVID-19 were assigned a group of severe cases requiring intubation and intensive care treatment (CoV_sev, n=18) and a group of intermediate severity (CoV_int, n=20), in which patients were hospitalized and either required no oxygen or received noninvasive supplemental oxygen. Horowitz indices (Pao_2/Fio_2) of patients with CoV_sev were directly derived from ventilation parameters. For CoV_int, the Horowitz index was calculated from noninvasive oxygen support (Fio_2 approximation) and pulse oximetry (Pao_2 approximation).[18]

Flow Cytometric Phenotyping and Platelet/Coagulation Testing

Thirty-one patients with COVID-19, 5 patients with non–COVID-19 pneumonia, and 10 age-matched control patients without pulmonary pathology were included for flow cytometry, rotational thrombelastometry, and platelet function analyses. Baseline characteristics of the flow cytometric phenotyping and platelet/coagulation testing cohorts are detailed in Table I in the Data Supplement. Flow cytometric analysis was performed with blood from 11 patients with intermediate COVID-19 and from 5 patients with severe COVID-19, whereas platelet function testing, whole-blood impedance blood aggregometry, and rotational thrombelastometry were performed on blood from 9 patients with intermediate and 8 patients with severe COVID-19, with an overlap of 2 patients with severe COVID-19. To avoid batch effects, principle component analysis, t-Distributed Stochastic Neighbor Embedding (t-SNE)–based dimension reduction, and automated clustering were performed in n=7 controls, n=4 patients with non–COVID-19

pneumonia, n=5 patients with CoV_sev, and n=11 patients with CoV_int sampled and analyzed within 10 days.

Histopathologic Assessment

One patient, aged 91 years, showed a typical disease course, declined intensive care treatment, and was autopsied after developing progressive acute respiratory distress syndrome and succumbing to the infection on the 7th day after hospitalization (see details in Results and Figure 1A and 1B). For quantification of immunothrombosis/neutrophil extracellular trap formation (NETosis), lung specimens from 4 additional deceased patients with reverse transcriptase polymerase chain reaction–confirmed COVID-19 (age [median, 78; interquartile range, 69–86]); male [n=3, 60%]) were included, and 5 patients who had died of cardiovascular events without lung involvement. One lung autopsy specimen was from a deceased patient with COVID-19 who was also included in the flow cytometric phenotyping as a patient with severe COVID-19.

In Vitro Assays

We used peripheral blood from 3 additional patients who had reverse transcriptase polymerase chain reaction–confirmed COVID-19 requiring intensive care unit care (age [median,77; interquartile range, 67–81]; male [n=1, 33%]) and 5 healthy control patients, with an overlap of 1 control patient with the flow cytometric analysis, for in vitro analysis of platelet activation assay neutrophil isolation, assessment of steady-state activation, and induction of NETosis with platelet-rich plasma.

In accordance with the Declaration of Helsinki, and with the approval of the Ethics Committee of Ludwig-Maximilian-University Munich, informed consent of the patients or their guardians was obtained. Patients with COVID-19 are part of the CORKUM trial (COVID-19 Registry of the LMU University Hospital Munich; WHO trial ID DRKS00021225). Pseudonymized data were used for analysis; the study was approved by the ethics committee of LMU Munich (No: 20-245 and 19-274).

Histopathology

Histopathology and immunofluorescence stainings were performed on paraffin-embedded heart, lung, and kidney specimens of the autopsy specimen described in Figure 1. Hematoxylin-eosin and Van Gieson stainings were performed as previously described.[19] For immunofluorescence staining, specimens were deparaffinized and subsequently stained using a published protocol.[19] For histological quantification, we used 4 additional lung autopsy specimens from deceased patients who had COVID-19, and 5 lung autopsy specimens of patients deceased from cardiovascular events without lung involvement. The antibodies used were anti-myeloperoxidase (MPO), anti-citrullinated histone H3, anti-fibrinogen, anti-CD42b, and Hoechst 33342 for immunofluorescence, and anti-Fibrin and anti-CD42b for immunohistochemistry, as well. Slides were visualized using either Airyscan technology (Zeiss LSM 880), epifluorescence microscopy (Zeiss), or Vectra Polaris system. The 3-dimensional reconstruction was rendered with Imaris. For quantification of neutrophil extracellular traps (NETs) and microthrombi, blood vessels were defined as tubular or circular enclosed structures with 4′,6-diamidino-2-phenylindole–positive endothelial lining and visible elastica interna, and lack of ciliated epithelium and a lack of obvious communication with alveoli, as well. Intravascular cells were regarded as neutrophils if they stained positive for 4′,6-diamidino-2-phenylindole and MPO. NETs were defined as extracellular structures adjacent to MPO-positive neutrophils that stained MPO^{+} and $citH3^{+}$, and $4',6\text{-diamidino-2-phenylindole}^{int/high}$, as well. Vessels were considered to contain immunothrombotic occlusions if there was a (partial) occlusion of the vessel lumen that stained positive for a network of fibrinogen, neutrophils (MPO), and platelets (CD41; see Figure IIA in the Data Supplement). The mean of 3 high-power fields for each patient without massive lung damage or hepatization was used. Quantification was performed with ImageJ v2.0.0-rc-69.

Platelet and Neutrophil Phenotyping

Blood samples were obtained either from a peripheral vein or an arterial line. Two milliliters of patient blood was mixed with a Lysing-Paraformaldehyde-Fixation solution containing 300 µL heparin, 15.7 mL distilled water, and 2 mL FACS Lysing Solution 10× (BD Biosciences), containing formaldehyde and diethylene glycol. Blood was incubated for at least 1 hour to ensure complete virus inactivation and lysis of the red blood cells. Lysates were then centrifuged (400*g* for7 minutes) and the resulting pellets were resuspended in 400 µL phosphate-buffered saline containing 0.5% bovine serum albumin. Fifty microliters of the suspension was incubated with 50 µL of the antibody panel (Table II in the Data Supplement) for 20 minutes at room temperature. Measurements were performed on a BD LSRFortessa Flow Cytometer. Analysis was performed using FlowJo Software (FlowJo v. 10.6.1, BD).

After downsampling twice with Downsample v3 plugin and 2 concatenation steps, t-SNE of an equal and representative number of cells per group was performed using the t-SNE FlowJo plugin. Subpopulation detection was performed by applying the Phenograph algorithm (Phenograph Plugin for FlowJo)[20]; the resulting Phenograph clustering was then used to assign the neutrophil and platelet subpopulations. The principal component analysis and heat maps were created using the ClustVis algorithm.[21] All mean fluorescence intensities reported are relative mean fluorescence intensities (percent of maximum expression for particular marker) in arbitrary units. ClustVis heat map clustering was performed via correlation distance, average clustering with tightest cluster first for rows and Manhattan distance, and complete clustering and higher mean value first for columns or with no clustering for columns. Hyporeactive neutrophils were defined as decreased expression of naive-neutrophil marker L-selectin (CD62L), adhesion receptors CD11b and CD49d, and FcγRIII (CD16), as well. Exhausted platelets were defined as platelets that show a low expression of CD40L, and low activation marker exposure, as well.

In Vitro Assay

Blood from 3 patients with COVID-19 with severe disease (CoV_sev) and 5 control donors (Ctrl) was used for in vitro assays. Flow cytometric measurements were performed on a BD LSRFortessa Flow Cytometer. Analysis was performed using FlowJo Software (FlowJo v. 10.6.1, BD). Histological analysis was performed with ImageJ v2.0.0-rc-69.

Circulation. 2020;142:1176–1189. DOI: 10.1161/CIRCULATIONAHA.120.048488

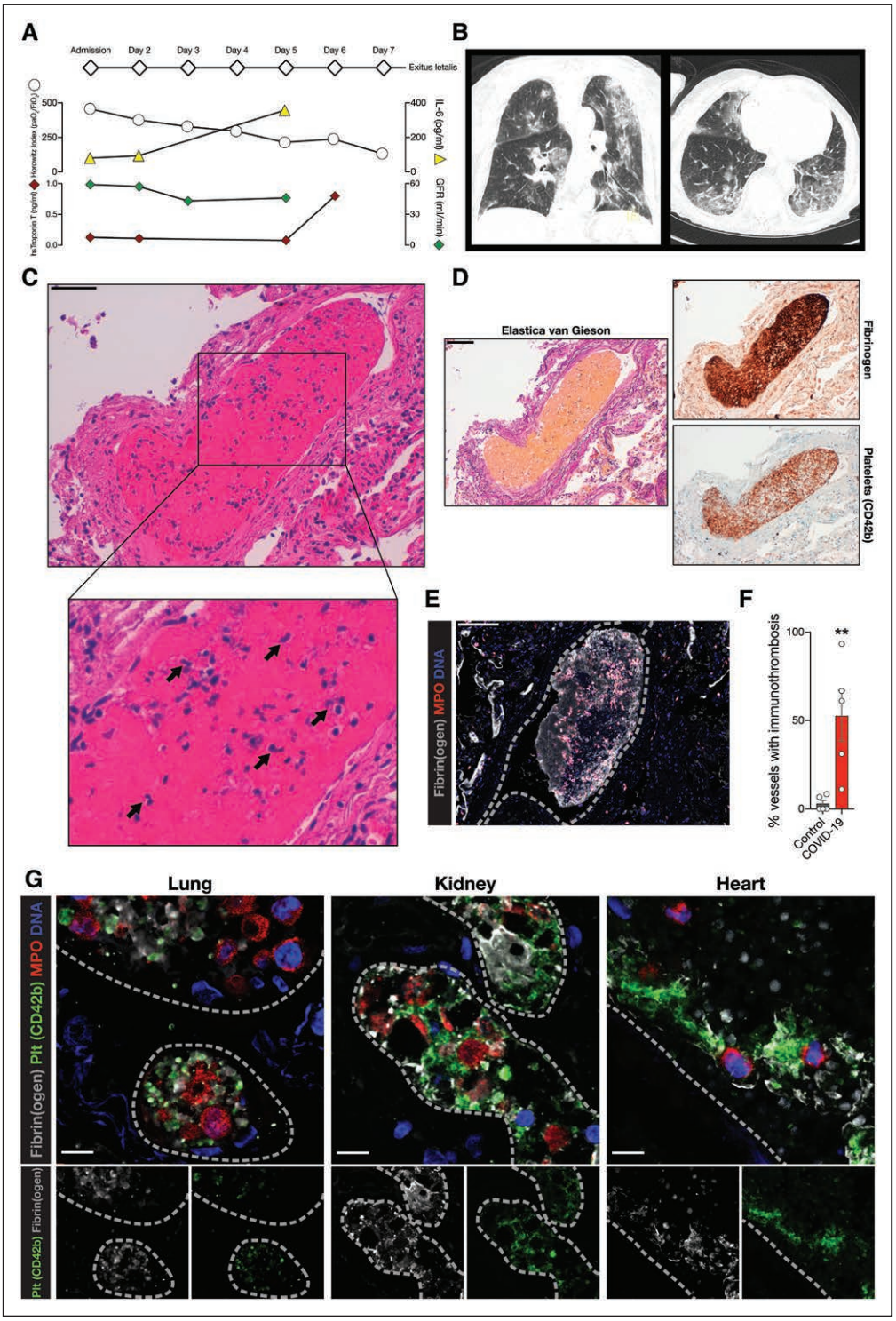

Figure 1. COVID-19–associated coagulopathy in the lung, kidney, and heart presents as microvascular immunothrombosis.
A, COVID-19 disease progression of autopsy case. Horowitz oxygenation index (Pao_2/Fio_2), and interleukin-6 (IL-6), high sensitive Troponin T and glomerular filtration rate (GFR) are plotted. **B**, Axial and coronal computed tomographic scans of the chest of the patient at presentation with COVID-19 defining bipulmonary infiltrates and ground glass opacities. **C**, Hematoxylin-eosin staining of a pulmonary microthrombus. Immune cells, most notably cells with segmented nuclei, can be observed in the thrombus (black arrows). **D**, Elastica van Gieson, fibrinogen, and platelet (CD42b) immunohistochemistry of the lung microthrombus. **E**, Exemplary immunofluorescence of a cut through a lung microthrombus showing of neutrophils (MPO) and fibrinogen. Dashed lines indicate vessel borders. Scale bars, 100 µm. **F**, Percentage of vessels with immunothrombosis (platelets, fibrinogen, neutrophils) in the lung vasculature. n=5 controls, n=5 COVID-19 autopsy cases. Two-tailed unpaired *t* test. **G**, Immunofluorescence staining of intravascular microthrombi with spatial association of neutrophils (MPO), platelets (Plt, CD42b) and fibrin. Scale bars, 10 µm; dashed lines indicate vessel borders. ****P*<0.01. COVID-19 indicates coronavirus disease 2019; and MPO, myeloperoxidase.

Platelet Activation Assay

Human platelets were isolated from citrated whole blood as described previously,[22] labeled antibodies against CD62P (BioLegend, Catalogue 304925) and PAC-1 (BioLegend, 362806), and subsequently exposed to Thrombin (0.01 and 0.1 U/mL), Convulxin (0.1 µg/mL), ADP (10 µmol/L), collagen (20 µg/mL), or NaCl (unstimulated) for 20 minutes at room temperature. After fixation with paraformaldehyde (1% final concentration), degranulation and integrin IIbIIIa activation were assessed by measuring mean fluorescent intensities of CD62P and PAC-1.

Neutrophil Isolation and Assessment of Steady-State Activation

Whole blood was drawn from patients with CoV_sev (n = 3) and healthy donors (n = 5) into EDTA-containing vials. Neutrophil granulocytes were isolated using magnetic beads (EasySep Direct Human Neutrophil Isolation Kit, Stemcell Technologies, Catalogue No. 19666) according to manufacturer's instructions. Isolated neutrophils were subsequently seeded onto Ibidi µ-Slides (VI 0.4) coated with poly-L-lysine (Sigma) by brief centrifugation (40*g*, 5 minutes), washed with phosphate-buffered saline 3 times, and then fixed with 1% Paraformaldehyde (10 minutes). Cells were permeabilized (0.5% Triton X-100, 10 minutes) and stained with anti-myeloperoxidase (MPO, R&D Systems AF3667), anti-citrullinated histone H3 (Abcam ab5103), and Hoechst dye for 30 minutes. Cells were visualized by immunofluorescence microscopy (6 fields of view at 40× magnification per replicate), and the number of activated neutrophils defined by citrullinated H3–positive nuclei, and extracellular citrullinated H3/MPO–positive foci, as well, were assessed.

Induction of NETosis With Platelet-Rich Plasma

Neutrophils from a healthy donor were isolated using a Ficoll-Paque gradient (GE Healthcare) according to the manufacturer's instructions and seeded onto Ibidi µ-Slides (VI 0.4) coated with poly-L-lysine (Sigma) by brief centrifugation (40*g*, 5 minutes). Platelet-rich plasma from 3 patients with CoV_sev and 5 healthy donors was isolated as described previously,[22] stimulated with 2.3 mmol/L calcium chloride and 20 µmol/L ADP and subsequently added to the seeded neutrophils for 20 minutes (37°C, 5% CO_2). Neutrophil-platelet aggregates were fixed with 1% Paraformaldehyde (10 minutes), permeabilized using 0.5% Triton X-100 (10 minutes), and stained with anti-MPO, anti-citrullinated H3, anti-CD41 antibodies (HIP8 clone, Biolegend), and Hoechst dye to counterstain nuclei. NETosis and neutrophil-platelet interaction were visualized by immunofluorescence microscopy (6 fields of view at 40× magnification per replicate). NETosis was defined according to the criteria mentioned earlier in the article (see Histopathology in Methods).

Neutrophil Activation Assay by Flow Cytometry

Fifty microliters of whole blood from CoV_sev (n = 3) and healthy controls (n = 5) were incubated with 2.3 mmol/L calcium chloride and 50 nmol/L phorbol myristate acetate or dimethyl sulfoxide (Ctrl), for 20 minutes at room temperature. Treated samples and an untreated control sample were incubated with an antibody panel for neutrophil activation (CD11b, CD62L, CD63, CD15; Biolegend) for 10 minutes, lysed and fixed with 400 FACS Lysing buffer and subsequently analyzed by flow cytometry (BD LSRFortessa Flow Cytometer, data analysis with FlowJo v. 10.6.1, BD).

Platelet and Coagulation Testing

Platelet and coagulation testing were performed in a subset of included patients. We used the Platelet Function Analyzer (INNOVANCE PFA 200 System, Siemens Healthineers) to assess platelet function under high-shear conditions, mimicking primary hemostasis in the arterial system. In brief, blood was flown through a cartridge containing a membrane either coated with collagen/epinephrine (PFA-EPI) or collagen/ADP (PFA-ADP). Platelet clotting was quantified by measuring closure times by standardized whole-blood impedance blood aggregometry (Multiplate Analyzer, Roche Diagnostics) to assess platelet function in hirudin-anticoagulated blood, excluding a contribution of fibrin formation in this setup. In brief, changes in impedance after addition of platelet agonists ADP and thrombin receptor activating peptide were used to assess platelet aggregation over time; the readout is standardized by assessing the area under the curve. In addition to standard international normalized ratio and activated partial thromboplastin time measurements, we performed enhanced analysis of platelet-coagulation interplay and clot formation under low-shear conditions using rotational thrombelastometry (Tem Innovations). This viscoelastic method allows the quantification of the dynamics and thrombus properties during clot formation and lysis. In brief, citrate-anticoagulated blood was recalcified and clot formation was initialized by adding start substances activating the intrinsic system (INTEM) or the extrinsic system (EXTEM). A possible effect of heparin was excluded by repeating the INTEM in the presence of heparinase (HEPTEM). To exclude platelet contribution to clotting, actin-inhibitor cytochalasin D was added to assess the soluble coagulation cascade in an isolated manner (FIBTEM).

All materials used were obtained from the manufacturer, and all the platelet/coagulation function testing was performed according to published standard protocol in an accredited laboratory setting according to DIN EN ISO 15189.

Data Analysis and Statistics

Data were analyzed using Excel v.16 (Microsoft) and Prism v. 8.3.0. (GraphPad) software. Three-dimensional reconstructions of z-stack data were performed using Imaris (Bitplane). The principal component analysis and heat maps were created using ClustVis (flow cytometric analysis for details). Adobe Illustrator was used to assemble the graphical illustrations. Results are shown as mean±SEM, unless otherwise indicated. For direct comparisons between 2 groups, unpaired, 2-tailed Student *t* tests were used, or, in the case of platelet and interleukin-6 time courses, paired *t* tests. For comparisons between groups either nonparametric Kruskal-Wallis tests or 2-way ANOVAs were used. A post hoc Dunn or Dunnett multiple comparisons test to the control column (Ctrl) was used. For clarity, only post hoc test results are displayed in the graphs. If the Kruskal-Wallis or ANOVA test showed a difference between groups without a significant post hoc test, a bar over the graph indicates the ANOVA/Kruskal-Wallis *P* value. *P* values of ≤0.05 are considered significant and denoted with *, ≤0.01 denoted with **, and ≤0.001 denoted with ***.

Individual patients are represented as dots, unless otherwise indicated. Reference ranges for laboratory values as used at the patient's hospital, if available, are shown as gray boxes. If there were different reference ranges for male and female patients, the mean of the 2 was taken as the reference range. For all regression analyses, black lines represent best-fit line, gray area the 95% confidence interval. r^2 and *P* values (slope nonzero) are shown in plots.

RESULTS AND DISCUSSION

We sought to explore tissue injury in COVID-19 by studying histopathologic autopsy specimens from a deceased patient with reverse transcriptase polymerase chain reaction–confirmed SARS-CoV-2 infection and typical findings of COVID-19 pneumonia on computed tomography scans. The patient developed progressive respiratory failure (Horowitz index, Pao_2/Fio_2 at admission: 457; 6 days later: 132, reference range >300), signs of cardiac injury without ECG evidence for macrovascular thrombosis (high-sensitive troponin T concentration 0.798 pg/mL, reference range <0.014 ng/mL), kidney failure (glomerular filtration rate 43 mL/min; glomerular filtration rate decrease from admission, 27%), and dysregulated coagulation (D-dimer 3.9 µg/mL, reference range <0.5 µg/mL) over the course of the disease (Figure 1A and 1B). Hematoxylin-eosin staining revealed the formation of microvascular clots in the lung in the absence of pulmonary embolism, similar to observations in lung samples of patients who had SARS-CoV-1 infection during the SARS epidemic 2003 (Figure 1C and 1D).[23] In addition to platelets and fibrin (Figure 1D), these thrombi contained large numbers of granulocytes (Figure 1C, inset).

We and others have shown that, under certain inflammatory conditions, platelets, neutrophils (polymorphonuclear cells [PMNs]), and the coagulation cascade team up to contain invading pathogens, a process termed immunothrombosis,[16,24] that can aggravate tissue damage by triggering vessel occlusion and hypoxia.[25]

To further explore the contribution of immunothrombosis to the pathogenesis of COVID-19, we used immunofluorescence to define the cellular and molecular composition of the microthrombi. We confirmed the presence of neutrophils in the microthrombi, embedded in the fibrin clot (Figure 1E). We verified this finding in an additional 4 COVID-19 cases. Here, we observed strongly increased numbers of granulocyte-containing thrombi in COVID-19 autopsies, in comparison with lungs from patients deceased because of nonpulmonary pathology (see Figure 1F and Figure IIa in the Data Supplement). Confocal microscopy revealed numerous intravascular neutrophils in close association with platelets and fibrin (Figure 1G). These neutrophil-enriched depositions were not restricted to the lung, but were also present in renal and cardiac microvessels (Figure 1G). This led us to hypothesize that dysregulated immunothrombosis driven by activated neutrophils and immunogenic platelets might contribute to organ injury and a systemic thrombogenic state in COVID-19.

We therefore assessed neutrophil dynamics and activation state in 2 hospitalized COVID-19 cohorts of defined disease severity: (1) severe cases requiring intubation and intensive care treatment (CoV_sev, n=19), and (2) a group of intermediate severity (CoV_int, n=20), which either required no oxygen or received noninvasive supplemental oxygen (Figure IA and IB in the Data Supplement). Severe cases showed higher peripheral neutrophil counts, correlating with the degree of lung injury as assessed by the Horowitz index (Figure 2A and 2B).

To gain insight into neutrophil activation patterns in COVID-19, we used a comprehensive high-dimensional flow cytometric activation marker analysis and subsequent t-SNE dimension reduction. Comparing non–COVID-19 pneumonia (Ctrl_pneu) and patients without signs of infection (Ctrl) with CoV_int and CoV_sev cases, we identified distinct activation states (Figure 2C and 2D, Table II in the Data Supplement, Figure IIB through IIE in the Data Supplement, and Methods). To characterize the markers responsible for the COVID-19 neutrophil phenotypes, we used unsupervised clustering and subsequent gating of 6 neutrophil polarization states (PMN1 to PMN6, Figure 2E and 2F and Figure IIIA through IIIC in the Data Supplement). We found the PMN3 subcluster to be significantly enhanced in CoV_int cases. This subcluster showed a decrease in naive-neutrophil marker L-selectin (CD62L), and adhesion receptors CD11b and CD49d.[26,27] Also, FcγRIII (CD16) expression, which negatively correlates with neutrophil apoptosis, was found to be downregulated (Figure 2F and Figure IIID in the Data Supplement).[27] Therefore, the PMN3 profile points to hyporeactive and apoptotic neutrophils in the circulation of patients with CoV_int, possibly reflecting the outcome of neutrophil recruitment and activation in the lung vasculature. In contrast, activation marker CD177 was globally upregulated in severe COVID-19 cases (Figure IIID in the Data Supplement), and the highly activated subpopulation PMN6 was overrepresented in CoV_sev (32.1±12.9% of neutrophils in CoV_sev, versus 8.8±3.3% in controls; Figure 2F). CD177 furthermore correlated significantly with pulmonary disease severity, underlining a potentially causative role of neutrophils (Figure 2G). Isolation and staining of peripheral blood neutrophils from patients with CoV_sev showed increased activation of these cells in the circulation in comparison with controls (Figure 2H). In line, in vitro stimulation of CoV_sev neutrophils with phorbol myristate acetate revealed a differential response with increased CD63 expression indicating granule release, and decreased expression of

ORIGINAL RESEARCH ARTICLE

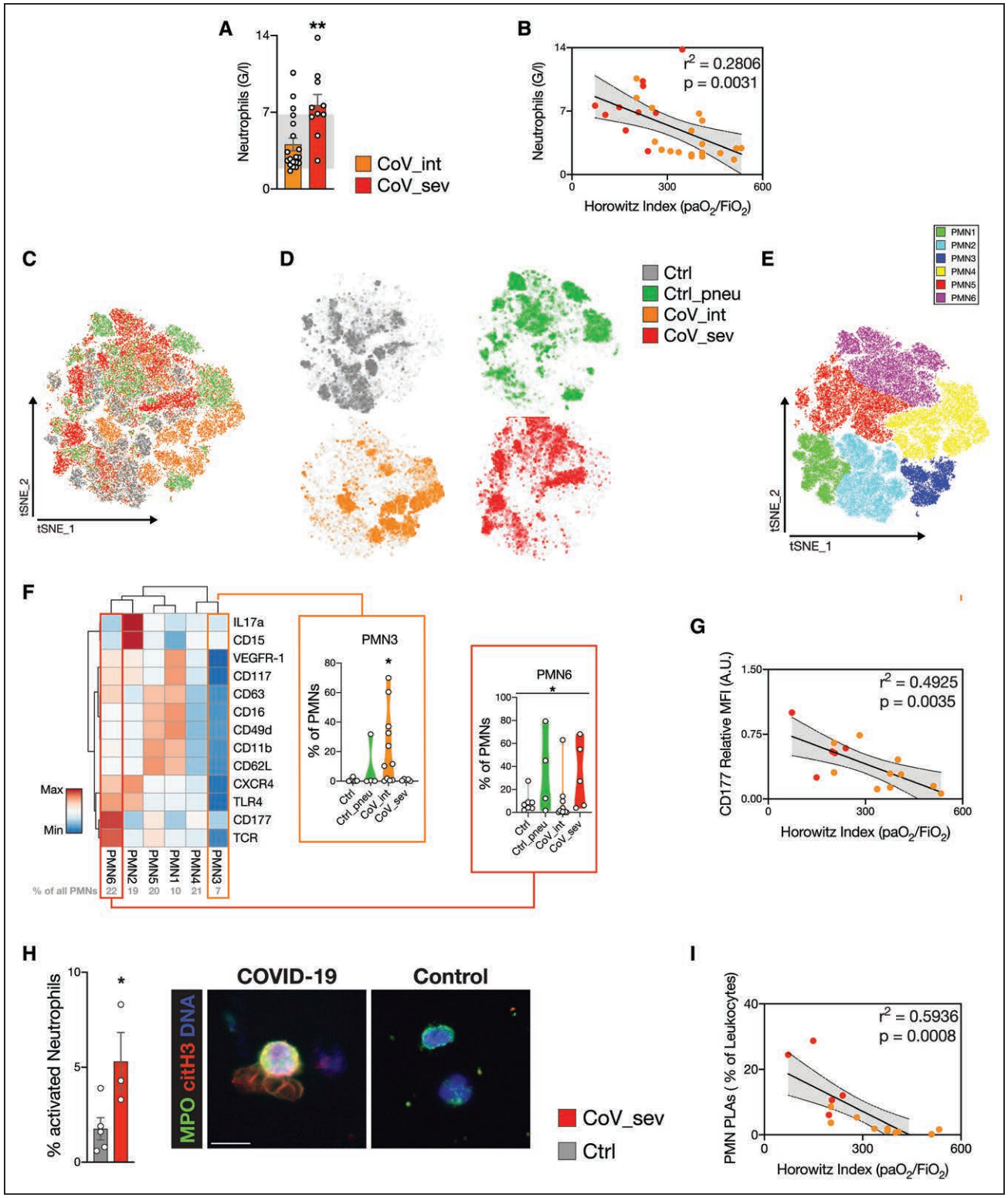

Figure 2. High-dimensional analysis of neutrophil markers reveals a distinct neutrophil signature, characterized by overshooting, global neutrophil activation in severe disease.

A, Neutrophil count of patients with COVID-19 from white blood cell differential: n=19 CoV_int, n=10 CoV_sev, 2-tailed unpaired Student *t* test. Reference range for neutrophil counts is shown in gray (1.85–6.8 G/L). **B**, Linear regression of neutrophil count with Horowitz index (Pao_2/Fio_2) of patients at blood draw. n=19 CoV_int, n=10 CoV_sev. **C** through **F**, t-Distributed Stochastic Neighbor Embedding (t-SNE) of neutrophil heterogeneity panel of Ctrl, Ctrl_pneu, CoV_int, and CoV_sev (n=25 000 downsampled cells per group). n=7 Ctrl, n=4 Ctrl_pneu, n=11 CoV_int, n=5 CoV_sev patients. **C**, t-SNE plot. **D**, t-SNE density plot displaying polarization of each group. **E**, Color-coded Phenograph-based subclusters of the t-SNE plot are shown. **F**, Heat map of the mean fluorescence intensity (MFI) for neutrophil subclusters relative to the maximum MFI. See Methods for the exact clustering of the heat map. For PMN 3 and PMN 6, (*Continued*)

Figure 2 Continued. the percentages of total neutrophils of each patient within this subcluster are annotated in violin plots. Percentages of neutrophils in each subcluster are shown in gray above the heat map. Kruskal-Wallis test and post hoc Dunn multiple comparison test. Line denotes significant Kruskal-Wallis test but nonsignificant post hoc test. **G**, Linear regression of CD177 expression of neutrophils with Horowitz index. n=10 CoV_int, n=5 CoV_sev. **H**, Percent of activated neutrophils in COVID-19 and control blood assessed by citH3 and MPO membrane blebbing in 6 high-power fields per patient. Representative micrographs are shown on the left. n=5 controls, n=3 CoV_sev. Two-tailed unpaired Student *t* test. **I**, Linear regression of neutrophil platelet aggregates as percentage of total blood leukocytes with Horowitz index. n=10 CoV_int, n=5 CoV_sev. **P*<0.05, ***P*<0.01. citH3 indicates citrullinated histone H3; COVID-19, coronavirus disease 2019; CoV_int, patient group with intermediate COVID-19; CoV_sev, patient group with severe COVID-19; Ctrl_pneu, non–COVID-19 pneumonia; MFI, mean fluorescence intensity; MPO, myeloperoxidase; and PMN, polymorphonuclear cells.

adhesion receptor CD11b in COVID-19 in comparison with controls (Figure IIIE in the Data Supplement). In summary, distinct neutrophil signatures exist in different courses of COVID-19 ranging from a hyporeactive phenotype in patients with intermediate COVID-19 to an excessive, global neutrophil activation characterizing severe COVID-19. Platelets are major initiators of neutrophil activation and boost neutrophil-driven tissue damage.[22] Indeed, in patients with COVID-19 formation of circulating platelet-neutrophil aggregates, a key element of immunothrombosis,[24] correlated in a linear fashion with pulmonary disease severity (Figure 2I).

Given the central role of platelets driving immunothrombosis,[22,28] we analyzed quantitative and qualitative changes of platelets. In COVID-19, thrombocytopenia at hospital admission is reported in more severe cases, hinting at platelet consumption.[29] In line with this notion, platelet counts in our cohort of patients with COVID-19 were at the lower end of the normal range (Figure 3A, Figure IVA in the Data Supplement). A longitudinal assessment of platelet counts revealed highly dynamic changes over time, in particular, in patients admitted to intensive care unit and requiring intubation (Figure 3B). When assessing individual platelet levels, 81% of patients with COVID-19 showed an increase (≥50%) during hospital stay (21/26 patients, Figure 3C), and 50% of patients even developed mild thrombocytosis (platelet count >360 000/µL, 13/26 patients). Interleukin-6 has been causally linked to thrombopoietin transcription and increased thrombopoiesis.[30] We correlated interleukin-6 plasma levels and platelet counts in patients with CoV_sev and CoV_int (Figure 3B). In severe cases, interleukin-6 peaked at the time of intubation/intensive care unit admission and was followed by a peak in platelet count with a lag of 5 days (Figure 3B and 3C). We observed a similar trend in the intermediate cohort (Figure IVB in the Data Supplement), indicating a link between the acute-phase inflammatory response and a reactive increase in platelet production in COVID-19.[31–33] Hematocrit levels of patients with CoV_int and CoV_sev decreased over the disease course, excluding dehydration as the reason for increased platelet count (Figure IVC in the Data Supplement).

To assess whether this quantitative shift in the platelet compartment was accompanied by phenotypic changes, we used comprehensive antibody-based surface marker analysis (Figure VA and VB in the Data Supplement, Table III in the Data Supplement, Methods). We performed t-SNE–based unsupervised clustering, which uncovered distinct changes in platelet marker profiles in intermediate and severe COVID-19 cases, in comparison with both patients with non–COVID-19 pneumonia and patients without signs of infection (Figure 3D and 3E and Figure VB in the Data Supplement). We confirmed this finding by using Principal Component Analysis, which revealed distinct platelet activation patterns with a strong correlation to disease severity (Figure VC and VD in the Data Supplement). To gain insight into these distinct marker profiles, we performed clustering of platelet populations in a robust manner (unsupervised clustering with Phenograph followed by subsequent supervised gating), defining 10 subclusters (platelet [Plt] 1–10[34]; Figure 3F and Figure VIA and VIB in the Data Supplement). Two of 10 identified subclusters were significantly enriched in CoV_int (Plt9 and Plt10), and 1 of 10 populations was enriched in CoV_sev (Plt4; Figure 3G, Figure VIB and VIC in the Data Supplement). All COVID-19–enriched clusters, and global expression analysis, as well (Figure VID in the Data Supplement), showed downregulation of scavenger receptor CD36 and transmembrane protein CD40L in comparison with control patients.

In patients with CoV_int, an expression heat map revealed generalized downregulation of platelet adhesion receptors, including CD41, CD31, and PSGL-1. In addition, Toll-like receptor 4 and C-X-C Motif Chemokine Receptor 4, which have been implicated in platelet host defense,[25] were decreased. In comparison with control cohorts, markers of platelet activation such as CD63, activated integrin GPIIbIIIa (PAC-1), and CD62P were downregulated or detected at similar levels in CoV_int (Figure VID in the Data Supplement).

In contrast, we identified a small but highly activated platelet population in some patients with CoV_sev (Plt1, 10.0% ±4.5 of platelets in CoV_sev, versus 3.1% ±0.7 in controls, Figure 3G). Plt4 subcluster, which was enriched in CoV_sev, showed low expression of GpIIbIIIa and CD36, comparable to CoV_int clusters, but exhibited a higher level of activation of immune receptors like CLEC-2 (Figure 3G), which also applied to the composite platelet heat map (Figure VD in the Data Supplement).

The overall hyporeactive phenotype in peripheral blood, in combination with evidence of recruitment to the pulmonary, renal, and cardiac microvasculature, suggested platelet activation within the microvasculature and subsequent circulation of exhausted platelets,

ORIGINAL RESEARCH ARTICLE

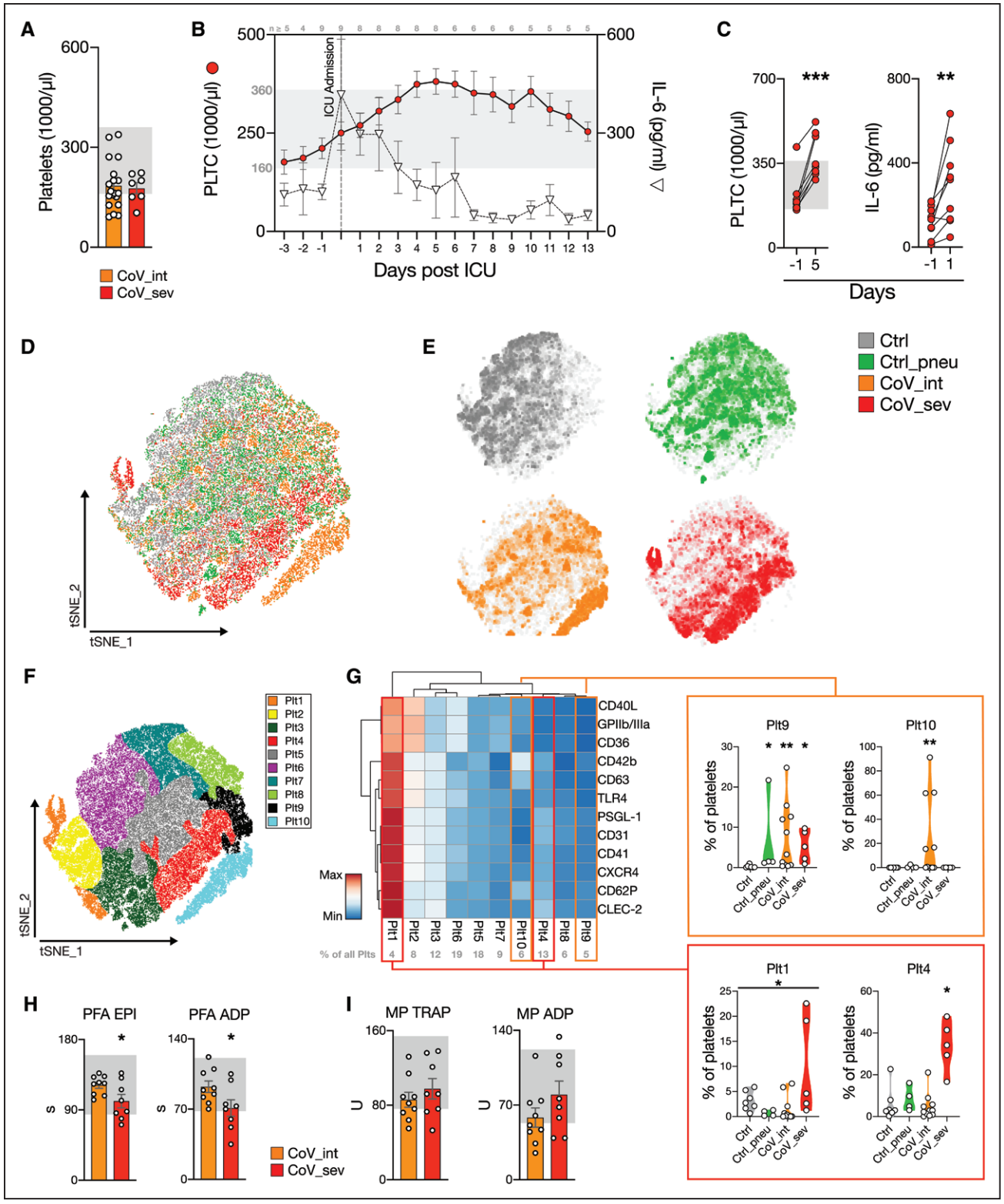

Figure 3. High-dimensional analysis of platelet markers and platelet function tests reveal a distinct platelet phenotype.
A, Platelet count on the day of admission for patients with intermediate (CoV_int n=19) and severe COVID-19 (CoV_sev n=7). Reference range for platelet counts is shown in gray (160–360 ×1000/µL). **B**, Time course of platelet count (red spheres) and interleukin-6 (IL-6; white triangles) of patients with CoV_sev normalized to the day of ICU admission. Number of patients for each time point shown above. Gray: reference range for platelet counts. **C**, Changes in platelet count and IL-6 measurements over time (days) in patients with CoV_sev. Gray: reference range for platelet counts (160–360 ×1000/µL). n=8 for PLTC, n=9 for IL-6. Two-tailed paired *t* test. **D**, t-Distributed Stochastic Neighbor Embedding (t-SNE) of platelet heterogeneity panel of Ctrl, Ctrl_pneu, CoV_int, and CoV_sev (n=40 000 downsampled cells per group). **E**, t-SNE plot displayed separately for each group, represented as a density plot. **F**, Color-coded Phenograph platelet subclusters. **G**, Heat map of the mean fluorescence intensity (MFI) for each platelet subcluster relative to the maximum MFI of the surface marker. (*Continued*)

Figure 3 Continued. See Methods for the exact clustering of the heat map. For subcluster population Plt 1, 4, 9 and 10, the percentages of total platelets of each patient within this subcluster are annotated in violin plots. Percentages of platelets in each subcluster are shown in gray above the heat map. Kruskal-Wallis test and a post hoc Dunn multiple comparison test. Line denotes significant Kruskal-Wallis test but nonsignificant post hoc test. **D** through **G:** n=7 Ctrl, n=4 Ctrl_pneu, n=11 CoV_int, n=5 CoV_sev patients. **H**, Platelet function analyzer-200 (PFA) results for collagen/epinephrine (EPI) and collagen/ADP (ADP). Gray: reference ranges for the PFA test (PFA EPI: 84–160 s PFA ADP: 68–121 s). n=9 CoV_int, n=8 CoV_sev, 2-tailed unpaired Student *t* test. **I**, Whole-blood impedance aggregometry (Multiplate, MP) results for thrombin-receptor agonist peptide (TRAP) and adenosine diphosphate (ADP) stimulation. Gray: reference ranges for the MP test (MP TRAP: 76–154 U, MP ADP: 53–122 U). n=9 CoV_int, n=8 CoV_sev. **P*<0.05, ****P*<0.01, ****P*<0.001. COVID-19 indicates coronavirus disease 2019; Ctrl_pneu, non–COVID-19 pneumonia; ICU, intensive care unit; and PLTC, platelet count.

in line with our data on neutrophils. Indeed, after activation and sequestration in the lung, exhausted platelets have been shown to recirculate in the blood.[35,36] Along these lines, lower CD40L densities known to mediate platelet-leukocyte interaction, and decreased scavenger receptor CD36 densities, as well, can be explained by activation and receptor shedding in the pulmonary vasculature.[37,38]

Because these data suggest a profound impact of COVID-19 on peripheral platelet function, we next assessed primary hemostasis under high-shear conditions using the PFA-200 system (Figure 3H, see Methods). Patients with CoV_int showed normal response to collagen-epinephrine, and to collagen-ADP matrices, as well. In CoV_sev, we found increased plug formation in both tests in comparison with CoV_int (Figure 3H). This might be caused by the aforementioned highly activated Plt1 subpopulation present in patients with CoV_sev.

Whole-blood impedance aggregometry showed mild reduction in platelet aggregation in COVID-19, with 41% of patients (7/17) below reference range after ADP stimulation (Figure 3I). This finding was mainly driven by hyporeactivity of CoV_int cases in response to ADP and thrombin-receptor agonist thrombin receptor activating peptide, with a less pronounced effect in CoV_sev. In a separate experiment, we measured platelet activation on stimulation with various agonists, which confirmed a dysregulated platelet phenotype in severe COVID-19, showing hyperreactivity toward weak agonists with a decreased maximal response toward strong agonists (see Figure VIE in the Data Supplement). In conclusion, platelet function analysis uncovered normal to (mildly) reduced platelet responses in CoV_int cases, in accordance with the hyporeactive platelet phenotype revealed by expression analysis. In patients with CoV_sev, we revealed a more complex activation pattern with signs of thrombogenic hyperreactivity and immunologic exhaustion.

Next, we defined whether changes in neutrophil and platelet activation are associated with changes in systemic plasmatic coagulation parameters in patients with COVID-19. In our cohort, international normalized ratio and activated partial thromboplastin time values were found to be within physiological range (Figure 4A). As previously published, patients with intermediate and severe COVID-19 exhibited elevated plasma fibrinogen, with almost 90% above reference range (27/31 patients, Figure 4B).[14] Fibrinogen levels correlated significantly with Horowitz index (Pao_2/Fio_2), a surrogate parameter for classification of acute respiratory distress syndrome severity (Figure 4C). Ferritin, another acute-phase protein previously described to be associated with COVID-19 severity, correlated to lesser extent (Figure VIIA in the Data Supplement). This could hint at a specific effect of SARS-CoV-2 on fibrinogen plasma levels beyond the canonical acute-phase response. Along these lines, the related strain SARS-CoV-1, the causative coronavirus in the 2003 SARS outbreak, was reported to directly upregulate fibrinogen expression in infected cells.[39]

We also found fibrin degradation product D-dimer to be strongly elevated in COVID-19 (mean 1.93 pg/mL), with 65% (13/20 patients) of CoV_int and all (11/11 patients) patients with CoV_sev above reference range (Figure 4D), pointing to constant activation of the coagulation cascade in patients with COVID-19. In addition, D-dimer also correlated significantly with disease severity (Figure VIIB in the Data Supplement).

Two important causes of elevated D-dimer are disseminated intravascular coagulation and macrovascular thrombosis, both complications of COVID-19.[15,40] However, normal to elevated platelet counts and elevated fibrinogen, in combination with normal activated partial thromboplastin time and international normalized ratio, excluded disseminated intravascular coagulation in our cohort. All patients with CoV_sev received prophylactic heparin treatment, and no event of macrovascular thrombosis (defined as stroke, myocardial infarction, or venous thromboembolism) was diagnosed at the time of enrollment in this closely monitored intensive care unit cohort,[15,41] suggesting microvascular (immuno) thrombosis as the possible culprit.

To more specifically assess platelet-coagulation interplay and clot formation under low-shear conditions, we used rotational thrombelastometry. Intrinsic (INTEM) and extrinsic (EXTEM) activation of clot formation revealed clot formation times (CFTs), maximal clot firmness (MCF), and clotting times within the reference range for nonsevere CoV_int cases (Figure 4E and 4F, Figure VIIC in the Data Supplement). Addition of heparinase (HEPTEM) to exclude a possible heparin-mediated effect showed similar MCF and CFT results (Figure VIID in the Data Supplement). However, in patients with CoV_sev, MCF was significantly increased, and CFT shortened in comparison with CoV_int (Figure 4E and 4F). INTEM and EXTEM clot formation correlated with neutrophil counts, and

ORIGINAL RESEARCH ARTICLE

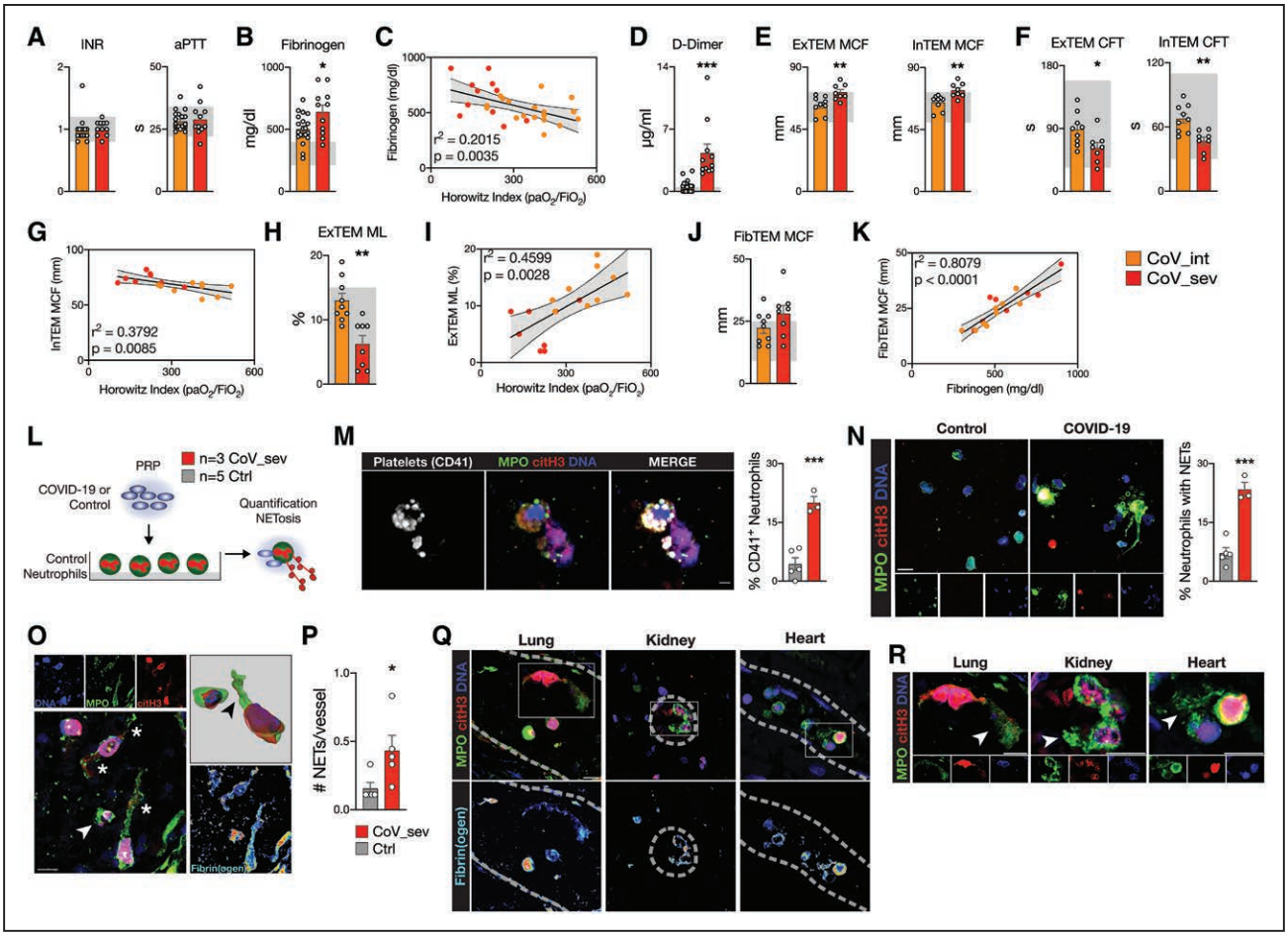

Figure 4. A systemic procoagulant state and neutrophil extracellular trap (NET) formation in COVID-19.
A, International normalized ratio (INR) and activated partial thromboplastin time (aPTT lupus anticoagulant-sensitive) of patients with COVID-19 at the time of blood draw. Reference ranges are shown in gray (INR, 0.8–1.2; aPTT, 22–34 s), n=19 CoV_int, n=11 CoV_sev. **B**, Fibrinogen (Clauss) plasma levels of patients with COVID-19 at the time of blood draw. Reference ranges are shown in gray (210–400 mg/dL), n=20 CoV_int, n=11 CoV_sev. **C**, Linear regression of fibrinogen plasma level and Horowitz index (Pao_2/Fio_2) of patients with COVID-19. n=19 CoV_int (orange), n=11 CoV_sev (red). **D**, D-Dimer plasma levels of patients with COVID-19. Reference ranges are shown in gray (<0.5 µg/mL), n=20 CoV_int, n=11 CoV_sev. **E**, EXTEM and INTEM maximum clot firmness (MCF). Reference ranges are shown in gray (EXTEM, 50–72 mm; INTEM, 50–72 mm) **F**, EXTEM and INTEM clot formation time (CFT). Reference ranges are shown in gray (EXTEM, 34–159 mm; INTEM, 30–110 mm). **G**, Linear regression of INTEM MCF and Horowitz index. **H**, EXTEM maximum lysis (ML). Reference ranges are shown in gray (<15%). **I**, Linear regression of EXTEM ML and Horowitz index. **J**, FIBTEM MCF, Reference ranges are shown in gray (9–25 mm). **K**, Linear regression of FIBTEM MCF and fibrinogen plasma levels. **E** through **K**, CoV_int n=9 and CoV_sev n=8. **E**, **F**, **H**, and **J**, Two-tailed unpaired Student *t* test. **L**, Schematic of the platelet-rich plasma (PRP) stimulation assay. **M**, Representative micrograph of platelets isolated from a patient with CoV_sev binding to a neutrophil undergoing NETosis in vitro and quantification of control or COVID-19 platelets associated with neutrophils (see **L**). Scale bar, 10 µm. **N**, Representative micrographs and quantification of NETs formed by neutrophils stimulated with control or COVID-19 PRP (see **L**). Scale bar, 20 µm. **M** and **N**, n=3 COVID-19 patients, n=5 controls. Two-tailed unpaired Student *t* test. **O**, Immunofluorescence staining of a representative COVID-19 lung autopsy specimen. Arrow indicate activated neutrophil; and Stars, neutrophil extracellular traps. **Top right**, Three-dimensional reconstruction if NETing neutrophil. Arrow indicates citH3 and DNA signal in MPO+ NET structure. **Bottom right**, pseudocolored fibrinogen costaining. Scale bar, 10 µm, dashed lines indicate vessel borders. **P**, NETs per vessels of COVID-19 and non–COVID-19 lung autopsy specimens. n=5 patients with COVID-19, n=5 controls. Two-tailed unpaired *t* test with Welch correction. **Q**, Immunofluorescence staining of COVID-19 autopsy specimens of the lung, kidney, and heart. **Top**, Staining for neutrophils (myeloperoxidase, MPO), DNA, and citrullinated histone H3 (citH3). Rectangles show areas of interest with NET-like structures in all 3 organs that are enlarged in **R**. **Bottom**, Fibrinogen staining is pseudocolored. Scale bar, 10 µm, dashed lines indicate vessel borders. **R**, Enlarged areas from **Q** with NET-like structures (arrows). Scale bar, 10 µm. **P*<0.05, ***P*<0.01, ****P*<0.001. CoV_int indicates patient group with intermediate COVID-19; CoV_sev, patient group with severe COVID-19; and COVID-19, coronavirus disease 2019.

disease severity, as well, exhibiting decreased CFT and increased clot firmness in more severe cases (Figure 4G and Figure VIIE through VIIG in the Data Supplement). Clotting time was within reference range and did not differ between CoV_int and CoV_sev, indicating that clotting factors are not the main drivers of the differences in MCF and CFT (Figure VIIC in the Data Supplement). After clot formation, maximum lysis of clots was also reduced in CoV_sev, and clot resistance to lysis correlated strongly with disease severity (Figure 4H and 4I).

Last, we excluded platelet contribution to clot formation by addition of actin polymerization inhibitor cytochalasin D. This revealed platelet-independent heightened plasmatic clot formation (FIBTEM) in severe and intermediate cases, with 53% above reference range for MCF (9/17 patients, Figure 4J). We hypothesized that increased clot formation might be, in

part, caused by the considerably elevated fibrinogen plasma concentrations in COVID-19. Indeed, plasma concentrations of fibrinogen and FIBTEM MCF correlated strongly in our cohort (Figure 4K), providing indirect evidence to this concept.

In summary, plasmatic coagulation is skewed toward a procoagulant state correlating with disease severity, reflected by peripheral blood coagulation tests, and histopathologic evidence of microvascular thrombosis in affected organs, as well.

Mechanistically, we uncovered dynamic quantitative and qualitative changes in neutrophil and platelet compartments in COVID-19, in addition to histopathologic and flow cytometric evidence of a partnership between these 2 cell types. Platelets are known to regulate neutrophil recruitment.[42] In particular, activated platelets have been shown to be critically involved in NETosis, a central element of immunothrombosis.[24,43,44] NETs have high procoagulant potential, and could therefore serve as a link to explain altered blood coagulation and microvascular thrombosis in SARS-CoV-2 infection.[45] Indeed, elevated markers of NETosis have been found in COVID-19, correlating with disease severity.[46]

To underline our hypothesis that partnership of neutrophils and dysregulated platelets drives NET formation and thereby possibly immunothrombosis in COVID-19, we superfused neutrophils isolated from healthy donors with activated platelet-rich plasma from either patients with CoV_sev or control patients (Figure 4L). Platelets from patients with severe COVID-19 showed increased adhesion to neutrophils (Figure 4M, Figure VIIIH in the Data Supplement), and resulted in enhanced NET formation, underlining the mechanistic link of immunogenic platelets driving neutrophil activation in COVID-19 (Figure 4N, Figure VIII in the Data Supplement).

Last, we reanalyzed tissue sections for the presence of microvascular NETs. Indeed, we discovered frequent intravascular NETs derived from neutrophils in the pulmonary vasculature, which were found to be virtually absent in control lungs (Figure 4O and 4P). NET-like structures were not only found in the pulmonary vasculature, but also in kidney and heart specimens (Figure 4Q and 4R). These structures were also spatially associated with fibrin deposition, underlining their procoagulant role (Figure 4O and 4P).

Taken together, we provide evidence that platelets, neutrophils, and the coagulation cascade are drivers of disease severity and might prove to be valuable pharmacological targets in COVID-19 (Figure VIII and Graphical Abstract in the Data Supplement). In addition, SARS-CoV-2–infected patients are at risk for increased thrombotic events, making prophylactic anticoagulation and vigilant monitoring for thrombotic complications a central task in the management of patients with COVID-19.

ARTICLE INFORMATION

Received May 6, 2020; accepted July 17, 2020.

The Data Supplement is available with this article at https://www.ahajournals.org/doi/suppl/10.1161/CIRCULATIONAHA.120.048488.

Authors

Leo Nicolai, MD; Alexander Leunig, BA; Sophia Brambs, cand med; Rainer Kaiser, MD; Tobias Weinberger, MD; Michael Weigand, MD; Maximilian Muenchhoff, MD; Johannes C. Hellmuth, MD; Stephan Ledderose, MD; Heiko Schulz, MD; Clemens Scherer, MD; Martina Rudelius, MD; Michael Zoller, MD; Dominik Höchter, MD; Oliver Keppler, MD; Daniel Teupser, MD; Bernhard Zwißler, MD; Michael von Bergwelt-Baildon, MD; Stefan Kääb, MD; Steffen Massberg, MD; Kami Pekayvaz, MD; Konstantin Stark, MD

Correspondence

Leo Nicolai, MD, or Kami Pekayvaz, MD, Medizinische Klinik und Poliklinik I, University Hospital Ludwig-Maximilian-University Munich, Marchioninistr. 15 81377, Munich, Germany. Email leo.nicolai@med.uni-muenchen.de or kami.pekayvaz@med.uni-muenchen.de

Affiliations

Medizinische Klinik und Poliklinik I (L.N., A.L., S.B., R.K., T.W., C.S., S.K., S.M., K.P., K.S.), Institute of Laboratory Medicine (M.W., D.T.), Medizinische Klinik und Poliklinik III (J.C.H., M.v.B.-B.), Department of Anesthesiology (M.Z., B.Z.), University Hospital Ludwig-Maximilian University Munich, Germany. DZHK (German Centre for Cardiovascular Research), partner site Munich Heart Alliance, Germany (L.N., A.L., R.K., T.W., C.S., S.K., S.M., K.P., K.S.). Virology, Max von Pettenkofer Institute (M.M., O.K.), Institute of Pathology (S.L., H.S., M.R.), Ludwig-Maximilian University Munich, Germany. German Center for Infection Research (DZIF), Partner Site Munich (M.M., O.K.). German Cancer Consortium (DKTK), Munich (J.C.H., M.v.B.-B.).

Acknowledgments

The authors thank the patients and their families for donating their blood and for their participation in the CORKUM registry. The authors also thank K. Lesser-Wetzold for her technical assistance and A. Titova for her help with histology. We thank all CORKUM investigators and staff. Authorship contributions: Initiation, Drs Nicolai and Leunig; Conceptualization, Drs Nicolai, Pekayvaz, and Stark; Methodology, Drs Nicolai, Pekayvaz, Leunig, S. Brambs, Rudelius; Investigation, Drs Nicolai, Pekayvaz, and Leunig, S. Brambs, Drs Kaiser, Weinberger, Weigand, Zwißler, Rudelius, Ledderose, Schulz, and Muenchhoff; Resources, Drs Massberg, Hellmuth, Scherer, Stark, Teupser, Keppler, von Bergwelt-Baildon, and Kääb; Formal Analysis, Drs Nicolai, Pekayvaz, and Leunig, S. Brambs, and Dr Kaiser; Writing – Original Draft, Dr Nicolai; Writing – Editing, all authors; Visualization, Drs Nicolai, Pekayvaz, and Leunig; Supervision, Drs Nicolai, Pekayvaz, and Stark; Project Administration, Drs Nicolai, Pekayvaz, and Stark; Funding Acquisition, Drs Nicolai, Pekayvaz, Massberg, and Stark.

Sources of Funding

This study was supported by the Deutsche Forschungsgemeinschaft (DFG) SFB 914 (to Dr Massberg [B02 and Z01], to Dr Stark [B02]), the DFG SFB 1123 (to Dr Massberg [B06], to Dr Stark [A07]), the DFG FOR 2033 (to Dr Massberg), the German Center for Cardiovascular Research (DZHK; Clinician Scientist Program [to Dr Nicolai], MHA 1.4VD [to Dr Massberg]), FP7 program (project 260309, PRESTIGE [to Dr Massberg]), FöFoLe project 1015/1009 (to Dr Nicolai), and the DFG Clinician Scientist Program PRIME (413635475, to Drs Pekayvaz and Kaiser). The work was also supported by the European Research Council (ERC-2018-ADG "IMMUNOTHROMBOSIS" [to Dr Massberg]).

Disclosures

None.

Supplemental Materials

Data Supplement Figures I–VIII
Data Supplement Tables I–III

REFERENCES

1. Zhu N, Zhang D, Wang W, Li X, Yang B, Song J, Zhao X, Huang B, Shi W, Lu R. A novel coronavirus from patients with pneumonia in China, 2019. *N Engl J Med.* 2020;82:727–733. doi: 10.1056/NEJMoa2001017
2. Zhou P, Yang XL, Wang XG, Hu B, Zhang L, Zhang W, Si HR, Zhu Y, Li B, Huang CL, et al. A pneumonia outbreak associated with a new coronavirus of probable bat origin. *Nature.* 2020;579:270–273. doi: 10.1038/s41586-020-2012-7
3. Ruan Q, Yang K, Wang W, Jiang L, Song J. Clinical predictors of mortality due to COVID-19 based on an analysis of data of 150 patients from Wuhan, China. *Intensive Care Med.* 2020;46:846–848. doi: 10.1007/s00134-020-05991-x
4. Wu Z, McGoogan JM. Characteristics of and important lessons from the coronavirus disease 2019 (COVID-19) outbreak in China: summary of a report of 72 314 cases from the Chinese Center for Disease Control and Prevention. *JAMA.* 2020;323:1239–1242. doi: 10.1001/jama.2020.2648
5. Cao B, Wang Y, Wen D, Liu W, Wang J, Fan G, Ruan L, Song B, Cai Y, Wei M. A trial of lopinavir–ritonavir in adults hospitalized with severe Covid-19. *N Engl J Med.* 2020;382:1787–1799. doi: 10.1056/NEJMoa2001282
6. Guan W-j, Ni Z-y, Hu Y, Liang W-h, Ou C-q, He J-x, Liu L, Shan H, Lei C-l, Hui DSC. Clinical characteristics of coronavirus disease 2019 in China. *N Engl J Med.* 2020;382:1708–1720. doi: 10.1056/NEJMoa2002032
7. Zhou F, Yu T, Du R, Fan G, Liu Y, Liu Z, Xiang J, Wang Y, Song B, Gu X, et al. Clinical course and risk factors for mortality of adult inpatients with COVID-19 in Wuhan, China: a retrospective cohort study. *Lancet.* 2020;395:1054–1062. doi: 10.1016/S0140-6736(20)30566-3
8. Cheng Y, Luo R, Wang K, Zhang M, Wang Z, Dong L, Li J, Yao Y, Ge S, Xu G. Kidney disease is associated with in-hospital death of patients with COVID-19. *Kidney Int.* 2020;97:829–838. doi: 10.1016/j.kint.2020.03.005
9. Guo T, Fan Y, Chen M, Wu X, Zhang L, He T, Wang H, Wan J, Wang X, Lu Z. Cardiovascular Implications of Fatal Outcomes of Patients With Coronavirus Disease 2019 (COVID-19). *JAMA Cardiol.* 2020;5:811–818. doi: 10.1001/jamacardio.2020.1017
10. Shi S, Qin M, Shen B, Cai Y, Liu T, Yang F, Gong W, Liu X, Liang J, Zhao Q, et al. Association of cardiac injury with mortality in hospitalized patients with COVID-19 in Wuhan, China. *JAMA Cardiol.* 2020;5:802–810. doi: 10.1001/jamacardio.2020.0950
11. Xu Z, Shi L, Wang Y, Zhang J, Huang L, Zhang C, Liu S, Zhao P, Liu H, Zhu L, et al. Pathological findings of COVID-19 associated with acute respiratory distress syndrome. *Lancet Respir Med.* 2020;8:420–422. doi: 10.1016/S2213-2600(20)30076-X
12. Wang T, Chen R, Liu C, Liang W, Guan W, Tang R, Tang C, Zhang N, Zhong N, Li S. Attention should be paid to venous thromboembolism prophylaxis in the management of COVID-19. *Lancet Haematol.* 2020;7:e362–e363. doi: 10.1016/S2352-3026(20)30109-5
13. Tang N, Bai H, Chen X, Gong J, Li D, Sun Z. Anticoagulant treatment is associated with decreased mortality in severe coronavirus disease 2019 patients with coagulopathy. *J Thromb Haemost.* 2020;18:1094–1099. doi: 10.1111/jth.14817
14. Han H, Yang L, Liu R, Liu F, Wu KL, Li J, Liu XH, Zhu CL. Prominent changes in blood coagulation of patients with SARS-CoV-2 infection. *Clin Chem Lab Med.* 2020;58:1116–1120. doi: 10.1515/cclm-2020-0188
15. Cui S, Chen S, Li X, Liu S, Wang F. Prevalence of venous thromboembolism in patients with severe novel coronavirus pneumonia. *J Thromb Haemost.* 2020;18:1421–1424. doi: 10.1111/jth.14830
16. Massberg S, Grahl L, von Bruehl ML, Manukyan D, Pfeiler S, Goosmann C, Brinkmann V, Lorenz M, Bidzhekov K, Khandagale AB, et al. Reciprocal coupling of coagulation and innate immunity via neutrophil serine proteases. *Nat Med.* 2010;16:887–896. doi: 10.1038/nm.2184
17. Engelmann B, Massberg S. Thrombosis as an intravascular effector of innate immunity. *Nat Rev Immunol.* 2013;13:34–45. doi: 10.1038/nri3345
18. Simon M, Wachs C, Braune S, de Heer G, Frings D, Kluge S. High-flow nasal cannula versus bag-valve-mask for preoxygenation before intubation in subjects with hypoxemic respiratory failure. *Respir Care.* 2016;61:1160–1167. doi: 10.4187/respcare.04413
19. Marx C, Novotny J, Salbeck D, Zellner KR, Nicolai L, Pekayvaz K, Kilani B, Stockhausen S, Bürgener N, Kupka D, et al. Eosinophil-platelet interactions promote atherosclerosis and stabilize thrombosis with eosinophil extracellular traps. *Blood.* 2019;134:1859–1872. doi: 10.1182/blood.2019000518
20. Levine JH, Simonds EF, Bendall SC, Davis KL, Amir el-AD, Tadmor MD, Litvin O, Fienberg HG, Jager A, Zunder ER, et al. Data-driven phenotypic dissection of AML reveals progenitor-like cells that correlate with prognosis. *Cell.* 2015;162:184–197. doi: 10.1016/j.cell.2015.05.047
21. Metsalu T, Vilo J. ClustVis: a web tool for visualizing clustering of multivariate data using Principal Component Analysis and heatmap. *Nucleic Acids Res.* 2015;43(W1):W566–W570. doi: 10.1093/nar/gkv468
22. Gaertner F, Ahmad Z, Rosenberger G, Fan S, Nicolai L, Busch B, Yavuz G, Luckner M, Ishikawa-Ankerhold H, Hennel R, et al. Migrating platelets are mechano-scavengers that collect and bundle bacteria. *Cell.* 2017;171:1368–1382.e23. doi: 10.1016/j.cell.2017.11.001
23. Ding Y, Wang H, Shen H, Li Z, Geng J, Han H, Cai J, Li X, Kang W, Weng D, et al. The clinical pathology of severe acute respiratory syndrome (SARS): a report from China. *J Pathol.* 2003;200:282–289. doi: 10.1002/path.1440
24. Clark SR, Ma AC, Tavener SA, McDonald B, Goodarzi Z, Kelly MM, Patel KD, Chakrabarti S, McAvoy E, Sinclair GD, et al. Platelet TLR4 activates neutrophil extracellular traps to ensnare bacteria in septic blood. *Nat Med.* 2007;13:463–469. doi: 10.1038/nm1565
25. Nicolai L, Gaertner F, Massberg S. Platelets in host defense: experimental and clinical insights. *Trends Immunol.* 2019;40:922–938. doi: 10.1016/j.it.2019.08.004
26. Silvestre-Roig C, Hidalgo A, Soehnlein O. Neutrophil heterogeneity: implications for homeostasis and pathogenesis. *Blood.* 2016;127:2173–2181. doi: 10.1182/blood-2016-01-688887
27. Dransfield I, Buckle AM, Savill JS, McDowall A, Haslett C, Hogg N. Neutrophil apoptosis is associated with a reduction in CD16 (Fc gamma RIII) expression. *J Immunol.* 1994;153:1254–1263.
28. Gaertner F, Massberg S. Patrolling the vascular borders: platelets in immunity to infection and cancer. *Nat Rev Immunol.* 2019;19:747–760. doi: 10.1038/s41577-019-0202-z
29. Lippi G, Plebani M, Henry BM. Thrombocytopenia is associated with severe coronavirus disease 2019 (COVID-19) infections: a meta-analysis. *Clin Chim Acta.* 2020;506:145–148. doi: 10.1016/j.cca.2020.03.022
30. Kaser A, Brandacher G, Steurer W, Kaser S, Offner FA, Zoller H, Theurl I, Widder W, Molnar C, Ludwiczek O, et al. Interleukin-6 stimulates thrombopoiesis through thrombopoietin: role in inflammatory thrombocytosis. *Blood.* 2001;98:2720–2725. doi: 10.1182/blood.v98.9.2720
31. Ishiguro A, Suzuki Y, Mito M, Shimbo T, Matsubara K, Kato T, Miyazaki H. Elevation of serum thrombopoietin precedes thrombocytosis in acute infections. *Br J Haematol.* 2002;116:612–618. doi: 10.1046/j.0007-1048.2001.03304.x
32. Schafer AI. Thrombocytosis. *N Engl J Med.* 2004;350:1211–1219. doi: 10.1056/NEJMra035363
33. Prina E, Ferrer M, Ranzani OT, Polverino E, Cillóniz C, Moreno E, Mensa J, Montull B, Menéndez R, Cosentini R, et al. Thrombocytosis is a marker of poor outcome in community-acquired pneumonia. *Chest.* 2013;143:767–775. doi: 10.1378/chest.12-1235
34. Reyes M, Filbin MR, Bhattacharyya RP, Billman K, Eisenhaure T, Hung DT, Levy BD, Baron RM, Blainey PC, Goldberg MB, et al. An immune-cell signature of bacterial sepsis. *Nat Med.* 2020;26:333–340. doi: 10.1038/s41591-020-0752-4
35. Cloutier N, Allaeys I, Marcoux G, Machlus KR, Mailhot B, Zufferey A, Levesque T, Becker Y, Tessandier N, Melki I, et al. Platelets release pathogenic serotonin and return to circulation after immune complex-mediated sequestration. *Proc Natl Acad Sci U S A.* 2018;115:E1550–E1559. doi: 10.1073/pnas.1720553115
36. Pareti FI, Capitanio A, Mannucci L, Ponticelli C, Mannucci PM. Acquired dysfunction due to the circulation of "exhausted" platelets. *Am J Med.* 1980;69:235–240. doi: 10.1016/0002-9343(80)90383-6
37. Tariket S, Hamzeh-Cognasse H, Laradi S, Arthaud CA, Eyraud MA, Bourlet T, Berthelot P, Garraud O, Cognasse F. Evidence of CD40L/CD40 pathway involvement in experimental transfusion-related acute lung injury. *Sci Rep.* 2019;9:12536. doi: 10.1038/s41598-019-49040-0
38. Werner JL, Steele C. Innate receptors and cellular defense against pulmonary infections. *J Immunol.* 2014;193:3842–3850. doi: 10.4049/jimmunol.1400978
39. Tan YJ, Tham PY, Chan DZ, Chou CF, Shen S, Fielding BC, Tan TH, Lim SG, Hong W. The severe acute respiratory syndrome coronavirus 3a protein up-regulates expression of fibrinogen in lung epithelial cells. *J Virol.* 2005;79:10083–10087. doi: 10.1128/JVI.79.15.10083-10087.2005
40. Tang N, Li D, Wang X, Sun Z. Abnormal coagulation parameters are associated with poor prognosis in patients with novel coronavirus pneumonia. *J Thromb Haemost.* 2020;18:844–847. doi: 10.1111/jth.14768
41. Klok FA, Kruip MJHA, van der Meer NJM, Arbous MS, Gommers DAMPJ, Kant KM, Kaptein FHJ, van Paassen J, Stals MAM, Huisman MV, et al. Incidence of thrombotic complications in critically ill ICU patients with COVID-19. *Thromb Res.* 2020;191:145–147. doi: 10.1016/j.thromres.2020.04.013
42. Sreeramkumar V, Adrover JM, Ballesteros I, Cuartero MI, Rossaint J, Bilbao I, Nácher M, Pitaval C, Radovanovic I, Fukui Y, et al. Neutrophils scan

for activated platelets to initiate inflammation. *Science.* 2014;346:1234–1238. doi: 10.1126/science.1256478
43. Castanheira FVS, Kubes P. Neutrophils and NETs in modulating acute and chronic inflammation. *Blood.* 2019;133:2178–2185. doi: 10.1182/blood-2018-11-844530
44. Brinkmann V, Reichard U, Goosmann C, Fauler B, Uhlemann Y, Weiss DS, Weinrauch Y, Zychlinsky A. Neutrophil extracellular traps kill bacteria. *Science.* 2004;303:1532–1535. doi: 10.1126/science.1092385
45. Gould TJ, Vu TT, Swystun LL, Dwivedi DJ, Mai SH, Weitz JI, Liaw PC. Neutrophil extracellular traps promote thrombin generation through platelet-dependent and platelet-independent mechanisms. *Arterioscler Thromb Vasc Biol.* 2014;34:1977–1984. doi: 10.1161/ATVBAHA.114.304114
46. Zuo Y, Yalavarthi S, Shi H, Gockman K, Zuo M, Madison JA, Blair CN, Weber A, Barnes BJ, Egeblad M, et al. Neutrophil extracellular traps in COVID-19. *JCI Insight.* 2020;5:e138999. doi: 10.1172/jci.insight.138999